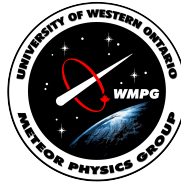




Department of Physics and Astronomy  
Ph.D. Astronomy with Collaborative  
Specialization in Planetary Science &  
Exploration



**Doctor of Philosophy's Thesis**  
**Statistical Characterization and Modeling of Meteoroid**  
**Ablation and Fragmentation Across Planetary Atmospheres**

August 28, 2023

Author:

Maximilian Vovk

Supervisor: Peter G. Brown  
Faculty of Science  
Western University



Statistical Characterization and Modeling of Meteoroid Ablation and  
Fragmentation Across Planetary Atmospheres  
Maximilian Vovk

## Contents

<b>1</b>	<b>INTRODUCTION</b>	<b>1</b>
1.1	Meteoroid Structure and Composition	2
1.2	Meteor Showers	4
1.3	Sporadic Meteors	5
<b>2</b>	<b>PLANETARY METEOR ENVIRONMENT</b>	<b>7</b>
2.1	Zodiacal Cloud Model	7
2.1.1	Earth	9
2.1.2	Mars	11
2.1.3	Venus	12
2.1.4	Titan	13
<b>3</b>	<b>METEOROID ABLATION MODELS</b>	<b>15</b>
3.1	Meteoroid single-body ablation models	16
3.2	Dust-ball Fragmentation Models	18
3.2.1	Thermal Disruption Model	19
3.2.2	Erosion Fragmentation Model	20
<b>4</b>	<b>PHD RESEARCH PROJECT</b>	<b>21</b>
4.1	Research Focus	21
4.2	Research Instrumentation	22
4.2.1	CAMO: Telescopic Observation System	22
4.2.2	EMCCD: Enhanced Meteor Imaging	23
4.3	Research Overview	24
4.3.1	Meteor Characteristics and Selection Criteria	24
4.3.2	Data Analysis and Model Development	24
4.3.3	Meteoroid Physical Characteristics Range	25
4.3.4	Interplanetary Application	26
4.4	Research Work Structure	26
4.5	Research Objectives	28
	<b>BIBLIOGRAPHY</b>	<b>28</b>

Statistical Characterization and Modeling of Meteoroid Ablation and  
Fragmentation Across Planetary Atmospheres

Maximilian Vovk



## List of Figures

Fig. 1–1:	Asteroid atmospheric impact frequency on Earth	1
Fig. 1–2:	Phases of meteoroid reentry	2
Fig. 1–3:	The selective ablation at different heights is a consequence of meteoroid minerals having different vaporization temperatures.	3
Fig. 1–4:	Dispersion of a meteoroid trail ejected by comet 21P/Giacobini-Zinner in 1900 [1].	4
Fig. 1–5:	The sporadic sources and Earth's interactions with them during its orbit around the Sun.	5
Fig. 2–1:	Zodiacal cloud and meteoroid size distribution in our solar system.	8
Fig. 2–2:	Bolides observed by Geostationary satellite GLM.	9
Fig. 2–3:	Terrestrial meteoroid influx based on the LDEF satellite data.	10
Fig. 2–4:	Neutral and ionic deposition rates of Mg, Fe, and Si on Mars.	11
Fig. 2–5:	Spirit image of a meteor streak over the Martian sky and Perseverance Martian Noctudile clouds.	12
Fig. 2–6:	Neutral and ionic deposition rates of Mg, Fe, and Si on Venus.	13
Fig. 2–7:	Neutral and ionic deposition rates of Mg, Fe, and Si on Titan.	14
Fig. 3–1:	Shape factor visualization for various forms.	17
Fig. 3–2:	Meteor showing terminal blending.	17
Fig. 3–3:	Comparison of Theoretical and Real Cometary Dust	19
Fig. 4–1:	Velocity distributions of meteoroids from JFC and MBA at 1 AU	21
Fig. 4–2:	Wide-field and Narrow-field CAMO cameras at Elginfield observatory.	22
Fig. 4–3:	Two EMCCD cameras at Elginfield observatory positioned at 70 deg and 40 deg elevations.	23
Fig. 4–4:	Mapping meteoroid mass to magnitude and flux	24
Fig. 4–5:	Charting selected events for study	25
Fig. 4–6:	Processing of a group of meteor events with PCA	26



Statistical Characterization and Modeling of Meteoroid Ablation and  
Fragmentation Across Planetary Atmospheres  
Maximilian Vovk

## List of Tables

Fig. 2–1:	In order minimum meteoroid entry velocities, escape velocity, planet orbit velocity and maximum meteoroid entry velocities of different solar system bodies.	8
Fig. 4–1:	Strategic division of tasks for the PhD project by semester.	27

## Acronyms

**CAMO** Canadian Automated Meteor Observatory

**DFN** Desert Fireball Network

**EMCCD** Electron Multiplying Charge-Coupled Device

**FPS** frames per second

**FRIPON** Fireball Recovery and Inter-Planetary Observation Network

**GLM** Geostationary Lightning Mapper

**HFC** Halley-family comet

**IDP** Interplanetary Dust Particle

**JFC** Jupiter-family comet

**LDEF** Long Duration Exposure Facility

**MAVEN** Mars Atmosphere and Volatile Evolution

**MBA** Main Belt asteroid

**MEM** Meteoroid Engineering Model

**NOAA** National Oceanic and Atmospheric Administration (NOAA)

**OCC** Oort cloud comet

**PMC** polar mesospheric cloud

**PR** Poynting–Robertson Effect

**WMPG** Western Meteor Physics Group

**WP** Work Packedges

**ZC** Zodiacal Cloud

**ZoDy** Zodiacal Cloud Dynamic Model

# 1 Introduction

Letters to Various Persons (ed. 1865)

*"New ideas come into this world somewhat like falling meteors,  
with a flash and an explosion."*

- Henry David Thoreau

Our solar system, with its diverse array of microscopic grains, asteroids, and planets, originated from the solar nebula approximately 4.5 Ga ago [2]. The material composition of these celestial bodies was influenced by their proximity to the Sun. Closer to the Sun, they primarily consist of iron and rock. However, beyond the solar ice line, the lower temperatures allowed for the solidification of more volatile substances such as water, carbon dioxide, ammonia, and carbon monoxide. These icy bodies, encompassing the Kuiper belt objects and Oort cloud comets, have played a pivotal role, possibly delivering life-essential elements to Earth as comets [3].

The asteroid belt, located between Mars and Jupiter, is home to remnants from the planetesimal phase. While these remnants could have potentially formed a planet, Jupiter's gravitational pull disrupted this process. As a result, the asteroid belt is populated by various-sized objects, from massive asteroids to tiny grains [2].

These remnants—asteroids and comets—provide a unique glimpse into the early stages of the solar system [2]. As Figure 1–1 shows, large celestial impacts on Earth are infrequent. However, Earth encounters numerous meteoroids daily—particles ranging from 1 m to 30  $\mu\text{m}$  in size [6]—amounting to 20 to 50 tons of material every day. These meteoroids, originating from asteroids and comets, become visible as meteors when they ionize the atmosphere during their passage, as shown in Figure 1–2. Only a select few reach the Earth's surface as meteorites [7]. Cameras capture these fleeting moments, helping researchers deduce their origins and characteristics [8].

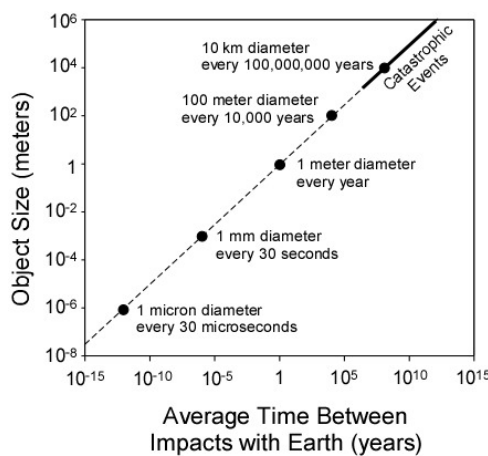
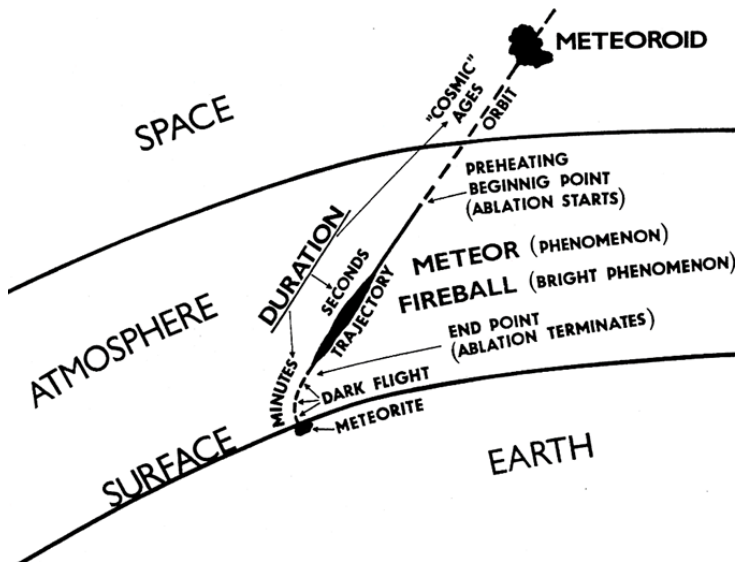


Fig. 1–1: Asteroid atmospheric impact frequency on Earth [4]



**Fig. 1–2: Phases of meteoroid reentry into the atmosphere [5]**

Understanding meteoroids, especially their material and structural attributes, is crucial for assessing satellite risks and studying meteoroid-atmosphere interactions [9].

This document outlines my proposed PhD research: a novel statistical model to characterize meteoroid structures based on recorded meteor events. This work is not only pivotal for satellite risk assessments, as it aids in the development of NASA’s Meteoroid Engineering Model (MEM) Version 4 but also benefits the broader scientific community.

The document provides a comprehensive overview of the current state of meteoroid research. In Section 1, we delve into meteoroids within the solar system, elucidating their structural properties and origins. Subsequent discussions in Section 2 explore the varying influences of meteoroids on distinct planets within our solar system. Section 3 offers an exposition on the evolution of meteoroid ablation models, with an emphasis on the specific model central to our investigation. Concluding, Section 4 outlines the dataset selected for this study and delineates our research trajectory for the forthcoming years.

## 1.1 Meteoroid Structure and Composition

The Earth’s surrounding meteoroid environment is primarily a product of asteroid fragments and cometary dust [10]. A significant portion of these meteoroids are chondrites, distinguished by their chondrules—millimeter-sized spherical bodies primarily composed of Si, Mg, and Fe from the early Solar Nebula [11]. The velocity range of these meteoroids upon entering Earth’s atmosphere is 11.2 km/s to 72 km/s, determined by their incoming speed and trajectory [12].

Given Earth’s near-circular orbit around the Sun at 30 km/s, objects with nearly parabolic orbits reaching perihelion at 1 AU exhibit velocities around 42 km/s. Thus, the maximum potential impact speed is 72 km/s when the objects move counter to Earth’s

direction. These objects, likely originating from highly eccentric cometary material, display porous compositions dominated by Mg-Fe-Si and CI-chondritic materials—rich in volatiles like water and organic matter, as evidenced by missions to comets like 1P/Halley and 81P/Wild 2 [11]. Typically, cometary material ablates quickly, leading to bright, short-lived meteors [8].

In contrast, objects entering the Earth-Moon system from the Sun's orbit, moving parallel to Earth's motion, approach Earth's atmosphere at the escape velocity of 11.2 km/s [2]. Such objects, predominantly from asteroidal orbits in the main belt, may also include old cometary materials shifted into low eccentric orbits by non-gravitational forces. These meteoroids generally ionize the atmosphere less compared to their faster counterparts, yielding dimmer meteors. Observations from space crafts like Hayabusa on asteroid Itokawa and Hayabusa 2 on Ryugu show these meteoroids are denser than cometary dust but more porous than terrestrial meteorites [8].

During ablation, vaporization of meteoroid materials releases ions that emit light in distinct spectral lines, contributing to understanding their composition [14]. Most lines originate from elements like Na I at 589 nm, Mg I at 518 nm, and Fe I between 527 – 545 nm [11]. Chondritic meteoroids are primarily silicate-based, however, Si is challenging to measure accurately, especially in fast meteoroids [14]. The line intensity varies based on the ablation temperature, as illustrated in Figure 1–3.

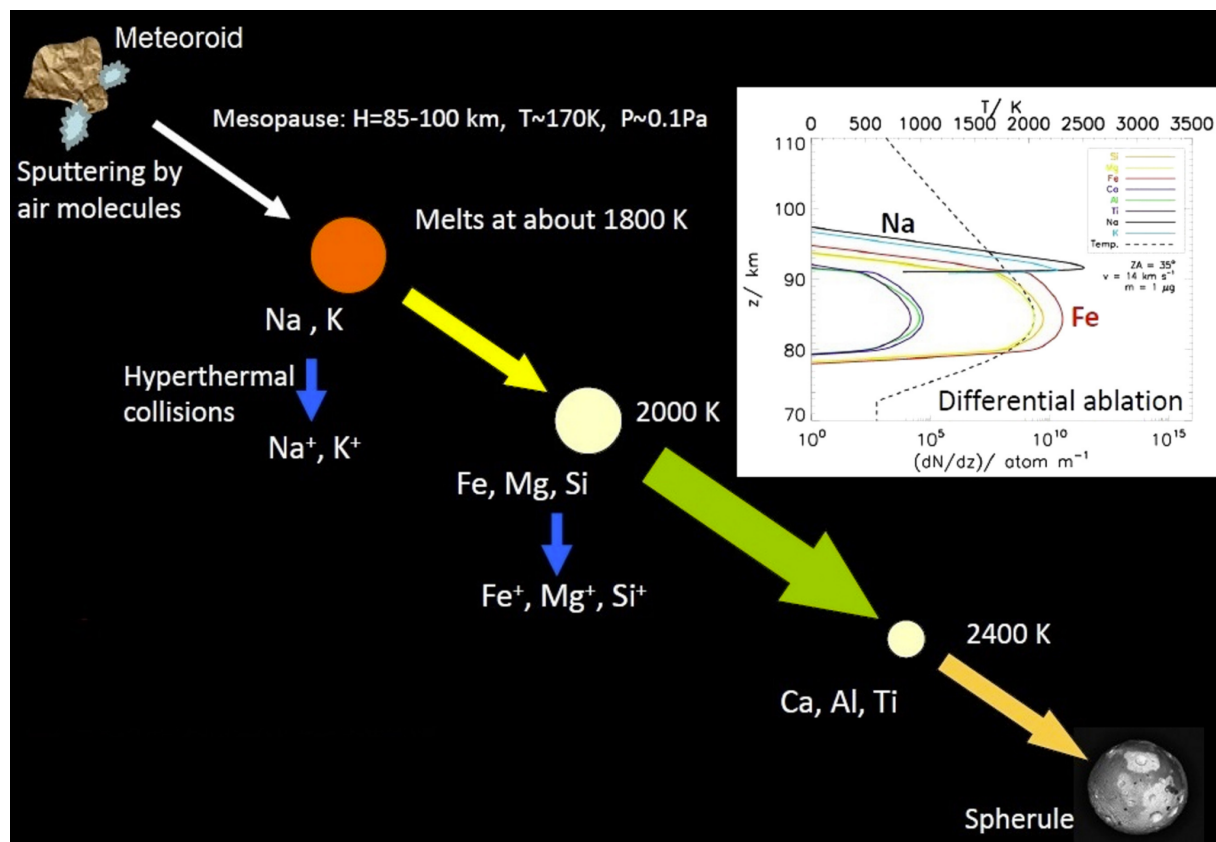


**Fig. 1–3:** The selective ablation at different heights is a consequence of meteoroid minerals having different vaporization temperatures [13].

Meteoroids with perihelion distances under 0.2 AU usually display sodium-depleted spectra due to evaporation from close solar proximity [11]. In contrast, Na-rich spectra are less common and suggest fresh cometary origins [14].

Meteors classified as "Irons" predominantly show Fe spectra. Although rare, accounting for only 4% of all falls, they represent about 20% of the mm-sized sporadic meteoroid population moving below 15 km/s [15]. These iron-dominant meteoroids differ in terms of ablation height and luminosity compared to their counterparts [16]. Meteoroids poor in Fe are likely cometary, deduced from their orbits and elevated entry altitudes, indicating a fragile structure [11].

## 1.2 Meteor Showers

Asteroids and comets can release material due to various mechanisms: the outgassing of vaporized material, tidal disruptions, or collision events. This released material, which consists of dust and fragments, continues on orbits similar to their parent bodies, forming what's known as a meteoroid stream. Notably, meteoroids from significant showers generally have mainstream compositions [11].

Depending on their size, these fragments experience various perturbing forces, such as radiation pressure, Poynting–Robertson Effect (PR) drag, sublimation, mutual collisions, and the dynamical effects of planets [17]. These forces spread the meteoroid stream and can cause variations in their orbital elements.

When such meteoroid streams intersect with Earth's atmosphere, they produce a meteor shower. Though these meteoroids enter the atmosphere on parallel trajectories, from an Earth-based observer's perspective, they appear to radiate from a single point in the sky. This point is known as the meteor shower's radiant, an effect due to the local

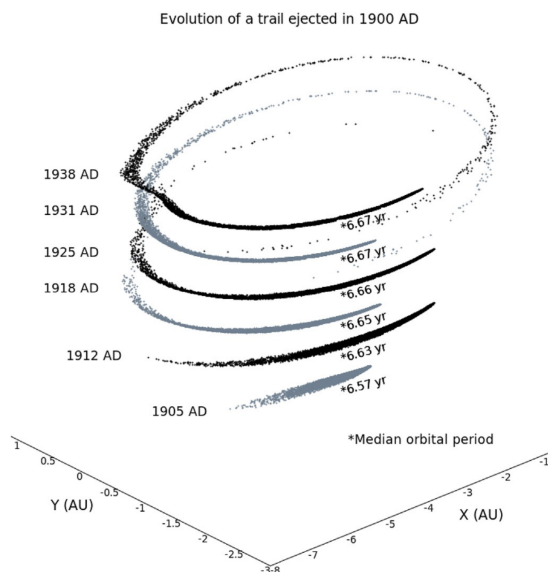


**Fig. 1–4: Dispersion of a meteoroid trail ejected by comet 21P/Giacobini-Zinner in 1900 [1].**

topocentric frame [18].

Meteor showers have distinct periodicities based on when Earth intersects with the stream. Examples include the Perseids in mid-August and the Geminids in mid-December. However, the intensity of these meteor showers can vary over the years, due to the dynamic evolution of the particles within the meteoroid stream [1], as depicted in figure 1–4.

### 1.3 Sporadic Meteors

The majority of meteors are not part of any specific meteor shower and are termed sporadic meteors. As the maximum hourly rate of meteor showers drops below 2 per hour, distinguishing them becomes a challenge. Over time, these meteor streams become sparse and blend with the interplanetary dust ubiquitous in our solar system. Consequently, they become part of the solar system's Zodiacal Cloud (ZC). As Earth orbits the Sun, it encounters these particles, as illustrated in figure 1–5. These particles predominantly lie in the lower velocity ranges, typically impacting Earth at velocities between 11.2 km/s and 20 km/s [17].

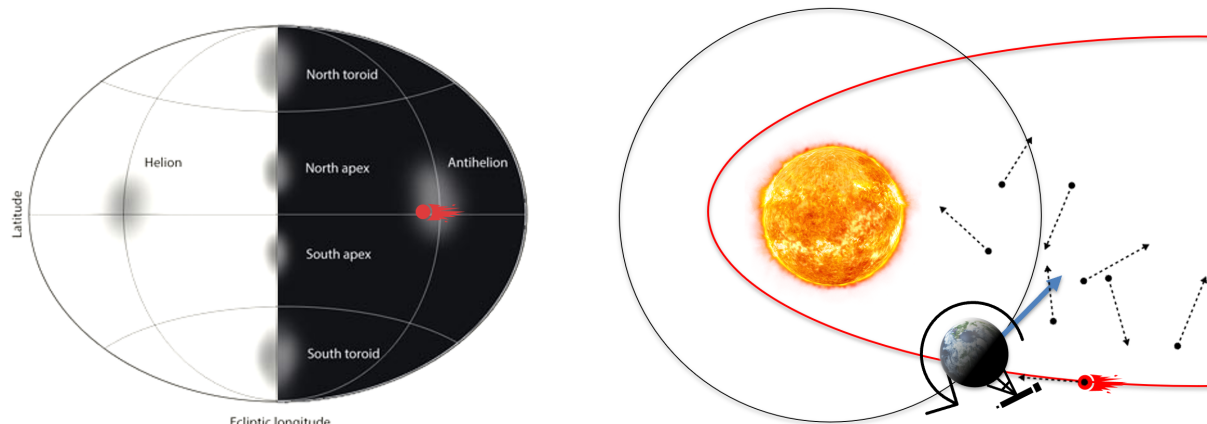


**Fig. 1–5: The sporadic sources and Earth’s interactions with them during its orbit around the Sun.**

Depending on their orbital characteristics, meteoroids can be categorized into:

- Short-period cometary orbits, or Jupiter-family comet (JFC) orbits, which have periods less than 20 years, exhibit low inclinations, and are significantly influenced by Jupiter’s gravity.
- Intermediate-period cometary orbits, or Halley-family comet (HFC) orbits, spanning orbital periods between 20 and 200 years and possibly exhibiting high inclinations.
- Long-period cometary orbits, or Oort cloud comet (OCC) orbits, which exceed 200-year orbital periods.
- Asteroidal orbits originating from Main Belt asteroids (MBAs).



## Introduction

The differentiation among these meteoroid orbits is often facilitated using Tisserand's parameter concerning Jupiter,  $T_J$ . Specifically, asteroidal orbits generally have  $T_J > 3$ , Jupiter-family cometary orbits fall between  $2 < T_J < 3$ , and long-period cometary orbits have  $T_J < 2$  [19].

The dominant mass contributors to the sporadic meteor environment are the Helion and Anti-Helion regions, aligned with the sun's central coordinate frame. Originating either from the side of Earth facing the Sun or its dark opposite, these regions predominantly host meteoroids from JFC and MBA orbits. For instance, meteoroids from the Anti-Helion region are depicted in red in figure 1–5. Compared to Anti-Helion meteoroids, those from the Helion region are denser, originating from older cometary material in JFC orbits and asteroidal material from MBA orbits [20]. The North/South Apex, the next most abundant source, comprises swift meteors with low inclinations, primarily from JFC and MBA orbits. Given their opposite trajectory to Earth's motion, they strike Earth at much greater speeds. Finally, the North/South Toroidal source includes high-speed meteors from highly inclined cometary orbits, such as HFC and OCC orbits, largely sourced from the Kuiper Belt [17].

## 2 Planetary Meteor Environment

From the fall of Rome to the middle ages, classical literature is replete with references to very bright meteors. In that epoch, reports of meteors were analogous to the alleged UFO sightings of today; most believed that those who claimed to have witnessed them fall from space were being untruthful. Such events were typically attested to by mere dozens of observers, often in remote, isolated locations. However, the sight of over 3000 fragments plummeting near L'Aigle in Normandy in 1803 presented undeniable evidence of celestial activity. The French Academy of Sciences dispatched Jean-Baptiste Biot to scrutinize this anomaly. Biot's subsequent report postulated the extraterrestrial origins of these fragments, laying the groundwork for meteoritics [21].

Our approach has since evolved from starry-eyed conjecture to rigorous data analysis. Terrestrial meteor events are regularly recorded both by amateurs and professional astronomers using specialized camera networks. These recordings deepen our understanding of the interactions between these celestial objects and our atmosphere upon entry [5].

Despite our extensive knowledge about terrestrial meteors, there's limited observational data concerning meteors on other planets. The first definitive observation of an extraterrestrial meteor in our solar system was when Comet Shoemaker-Levy 9 collided with Jupiter's atmosphere in July 1994. The comet, which was about 1.8 km in diameter, entered the atmosphere at a speed of 60 km/s, resulting in a brilliant fireball observed by multiple Earth observatories and satellites, including the Hubble telescope, the Galileo, and the Voyager 2 probe [22]. Such sizable meteor events are infrequent, rendering most meteors on other planets elusive due to their fainter appearances.

Research indicates that the Kappa Cygnids meteor stream passes in close proximity to Venus, potentially causing intense meteor showers on the planet. Similarly, the Orionids might have a more pronounced presence on Mars than on Earth. Nevertheless, direct observations of meteor showers on these planets remain elusive [23].

Satellites and rovers on Venus or Mars have captured only a handful of meteor events, largely due to the limitations of their instruments. These sporadic meteoroids belong to the expansive circumsolar disk, the Zodiacal Cloud (ZC), comprising dust particles resulting from asteroid collisions and cometary activities [17].

### 2.1 Zodiacal Cloud Model

The Zodiacal Cloud Dynamic Model (ZoDy) describes the mass, velocity, and radiant distributions of meteoroids ranging in size from a few centimeters to tens of microns that impact planets and moons within our solar system. The distribution of these particles within the Zodiacal Cloud (ZC) is shaped by solar non-gravitational forces. One such force is the solar radiation pressure, which sunlight exerts on objects in space. For inner solar system particles with masses below  $m < 10^{-10}$  g, the force due to solar radiation pressure becomes significant relative to gravitational forces, causing these

particles to drift towards the outer reaches of the solar system. Moreover, particles having a high area-to-mass ratio, typically between  $10^{-5} < m < 10^{-10}$  g, are influenced by the Poynting-Robertson drag. This drag arises from the absorption of solar radiation on a particle's front side and its subsequent re-emission as thermal radiation from the opposite side. Over time, this leads to orbital deceleration, causing the particle's orbit to become more eccentric and eventually spiral inwards towards the Sun, potentially leading to its sublimation if it gets too close. These non-gravitational influences result in a distinct particle distribution within the ZC: the inner solar system mainly contains larger heavier particles, while the outer regions predominantly house smaller lighter particles [24], as illustrated in Figure 2–1.

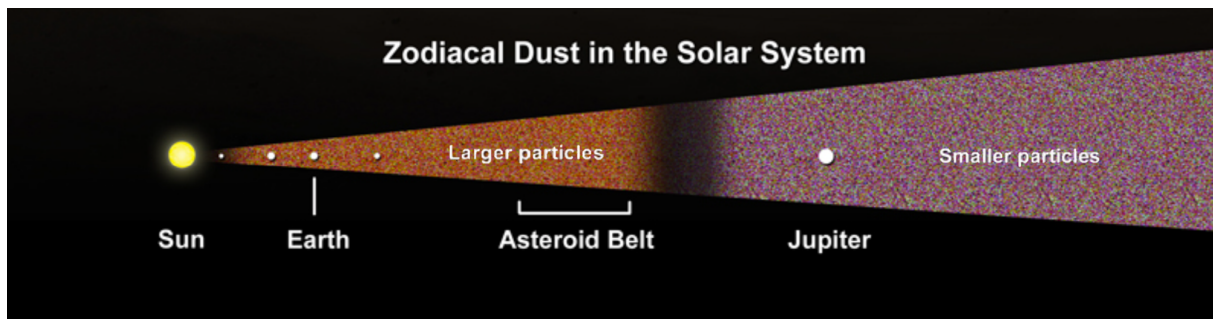


**Fig. 2–1: Zodiacal cloud and meteoroid size distribution in our solar system [25].**

Analyses from ZoDy indicate that the inner solar system is dominated by particles from JFC, MBA, and HFC orbits. While JFCs are the predominant mass contributors for the inner planets, the mass contribution from MBA particles becomes more pronounced closer to the main asteroid belt [26]. In the outer solar system, between Jupiter and Saturn, the Cassini spacecraft detected mostly JFC orbits in the interstellar dust particles. Moreover, the Pioneer 10 and 11 probes detected particles ranging between  $10^{-9}$  g and  $10^{-8}$  g up to 9.5 AU. Further out, Voyager 1 and 2 recorded a consistent presence of  $10^{-11}$  g particles originating from cometary orbits [27].

Meteors formed by ZC meteoroids vary based on the atmospheric density of the impacted planet, the meteoroid's entry velocity, and the gravitational field of the planet. The meteoroid's maximum and minimum entry velocity vary based on planetary bodies as detailed in Table 2–1.

**Tab. 2–1: In order minimum meteoroid entry velocities, escape velocity, planet orbit velocity and maximum meteoroid entry velocities of different solar system bodies [27].**

Planet	$V_{\min}$ [km/s]	$V_{\odot}$ [km/s]	$V_{\text{orb}}$ [km/s]	$V_{\max}$ [km/s]
Venus	10	50	35	85
Earth	11	42	30	72
Mars	5	34	24	58
Titan	2.6	13.7	5.58	29.1

Meteor influences on various planets have been documented, and multiple studies suggest that meteors play a substantial role across different planets.

### 2.1.1 Earth

The meteor environment of Earth is primarily dominated by sporadic sources in JFC orbits (accounting for 70%) and MBA orbits (9%). Meteors originating from HFC orbits or longer-period cometary orbits are comparatively rarer [26].

Meteors occur ubiquitously across Earth. This global distribution is illustrated in figure 2–2. A significant proportion of these events transpire over oceans and uninhabited areas. Additionally, many of these meteors occur during the day and therefore remain unseen [29]. Meteors exhibiting an absolute visual magnitude (at a distance of 100 km) of  $-4$  or brighter are termed as bolides or fireballs [6]. Terrestrial networks, such as Canadian Automated Meteor Observatory (CAMO), Fireball Recovery and Inter-Planetary Observation Network (FRIPON), and Desert Fireball Network (DFN), equipped with all-sky cameras, detect such phenomena. The NOAA Geostationary satellites, GOES-16 and GOES-17, also possess the capability to detect especially luminous bolides using the Geostationary Lightning Mapper (GLM) that primarily tracks lightning [30]. The high frame rate of this sensor (2 ms) facilitates the observation of both lightning and fireballs, specifically detecting the ionization frequency of oxygen at 777 nm [31]. Typically, the bolides spotted by these methodologies range from 0.1 m to 3 m in size, and events of this magnitude occur once or twice every few weeks [28].

Most meteors illuminating our skies are minuscule, often ranging between millimeters to centimeters in diameter. These produce faint streaks of light, predominantly falling within the  $-1$  to  $4$  magnitude range. Instruments like optical sensors and radars ef-

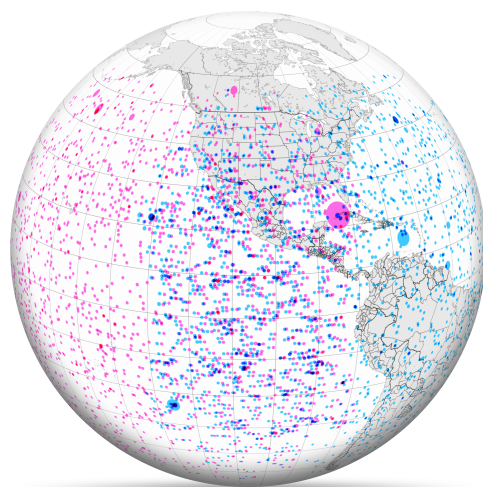


**Fig. 2–2:** Bolides observed by the Geostationary satellite GLM between July 23, 2017, and January 17, 2022, from GOES-16 and GOES-17. Events observed in stereo are highlighted in blue [28].



fectively detect these meteors [32]. Situating between 80 to 100 km altitude in the mesosphere, the peak occurrence is observed between 85 to 95 km [27].

Within the spectrum of meteoroid sizes, micrometeoroids play a pivotal role. These tiny meteoroids, primarily within the size range of micrometers, possess a significant area-to-mass ratio. As a result, they often melt into small globules with minimal mass loss. Notably, Interplanetary Dust Particles (IDPs)—particles below  $30 \mu\text{m}$  in size [6]—neither reach incandescence nor disintegrate, softly descending onto the Earth's surface [11]. These are often collected from various locations ranging from the poles to building rooftops globally.

Numerous satellites in Earth's orbit are continually bombarded by these particles, affecting satellite risk assessments. The Long Duration Exposure Facility (LDEF) satellite, orbiting between altitudes of 480 and 331 km, has provided valuable insights into the terrestrial meteoroid influx, as illustrated in figure 2–3 [33].

Every day, approximately 20 to 50 tons of micrometeoroid material pierce through our atmosphere [34]. These meteoroids, via the ablation process, significantly contribute to the metal content of the upper atmosphere. In the mesosphere, between 80 and 105 km, these meteoroids spawn the sodium (Na) layer of our atmosphere [35]. Furthermore, between 76 to 85 km, they act as nucleation centers for water ice crystals, giving birth to the noctilucent clouds, also known as polar mesospheric clouds (PMCs) [36]. Descending further, between altitudes of 12 to 30 km, these materials influence the aerosol composition and ozone chemistry of the stratosphere [35]. Meteorites accumulating to nearly 40 ktons annually enrich the Earth's surface. They play an essential role in nourishing the marine ecosystem, supplying free iron in remote oceanic domains, thus stimulating the very foundation of the marine food chain [37].

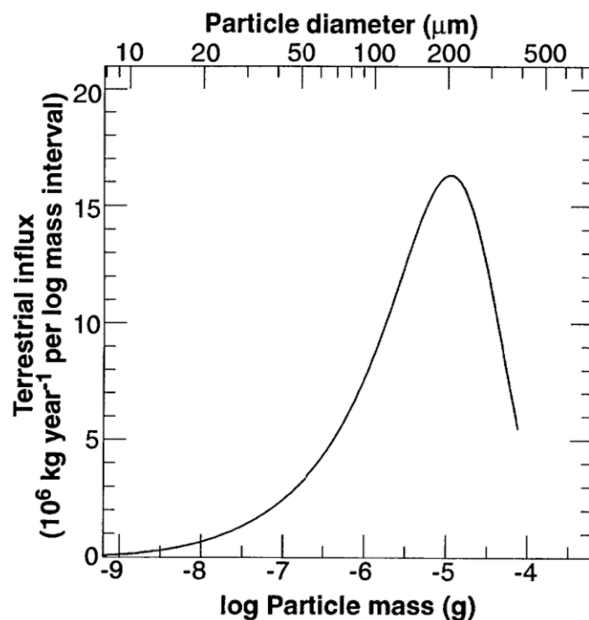


**Fig. 2–3:** Terrestrial meteoroid influx, as derived from the LDEF satellite data [33].

### 2.1.2 Mars

Located at 1.5 astronomical units (AU) from the sun, Mars is the smallest of the eight planets boasting an atmosphere. Its relative proximity to the sun yields a meteoroid environment comparable to that of Earth, predominantly characterized by JFC (accounting for 52%) and a heightened presence of MBA (14%) due to Mars's close orbit to the asteroid belt. Notably, the meteoroid mass on Mars is less than on Earth, with a daily influx of meteoroid material estimated at  $2.1 \pm 1.0$  t from the ZC [38].

Mars's atmosphere is overwhelmingly comprised of CO<sub>2</sub> (96%). Its atmospheric pressure, at 0.00628 atm, is analogous to Earth's at an altitude of 120 km [2]. While this altitude on Earth would initiate the ablation of most small meteoroids, the Martian atmosphere's lower density permits much larger particles, ranging from 60 to 1200  $\mu\text{m}$  in diameter, to withstand the atmospheric ablation phase and potentially reach the surface unmelted [39]. Meteors on Mars are typically produced by meteoroids of approximately 5 mm in diameter [40]. Preliminary estimates and simulations suggest that Mars would witness half the number of meteors visible on Earth of the same magnitude, with the majority of Martian meteors occurring at altitudes between 50 to 90 km [41]. These meteors are believed to achieve peak magnitude between altitudes of 75–85 km [27].

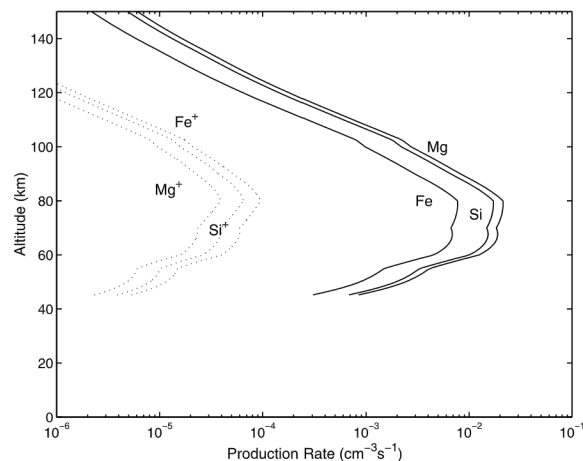


**Fig. 2–4: Neutral and ionic deposition rates of Mg, Fe, and Si on Mars [27].**

On Mars, Mg and Fe ions released during the ablation phase predominantly exchange charges with O<sub>2</sub><sup>+</sup>, resulting in Fe<sup>+</sup>O in the atmosphere. In contrast, neutral metals primarily react with O<sub>3</sub> before subsequently interacting with the abundant CO<sub>2</sub>, thus forming stable carbonated metallic atoms [27]. These compounds constitute the Martian ionospheric metallic layers, as depicted in figure 2–4. Such ionospheric layers, associated with meteoroid activity on Mars, have been observed by various satellites including Mariner IV, Mars 4 and 5, Mars Express, and Mars Atmosphere and Volatile Evolution (MAVEN) [38].

The Spirit Mars rover captured the first-ever detected meteor from another planet in 2004 [42]. This seminal discovery, presented in figure 2–5, has since been followed by only a dozen more observed meteors. However, some of these instances might be

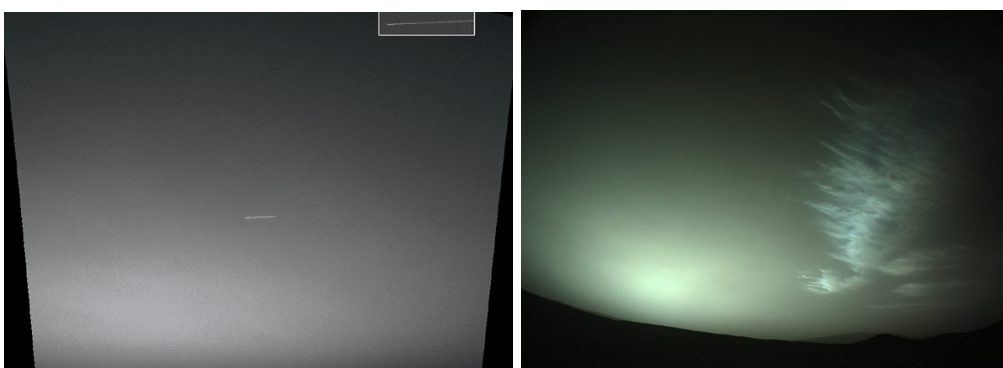


**Fig. 2–5:** On the left, Spirit image of a meteor streak over the Martian sky; on the right, Perseverance rover’s capture of Martian Noctilucent clouds.

attributed to cosmic rays impacting the camera’s detector [43].

Although distinct from Earth’s, Mars’s meteoroid environment does showcase some similar meteor proxies. Noctilucent clouds, for instance, nucleate around meteoric smoke particles on Earth. Analogous clouds have been identified on Mars from both satellite and rover observations (figure 2–5). Further data from the Mars Express and MAVEN satellites has revealed ionized metallic layers at 80–90 km altitudes, coinciding with the expected ablation heights for Martian meteoroids. These findings suggest a potential link between the observed spatial distribution of dry ice clouds on Mars and meteor activity [44].

The Mars Express mission has also confirmed the presence of a sporadic metal layer comprising magnesium and iron ions between altitudes of 65 and 110 km. This layer exhibits temporal variations [27]. While some postulate these fluctuations to be indicative of meteor showers stemming from cometary passages near Mars, others hypothesize that they might arise from impact ionization due to penetrating solar wind ions, as previously observed in proton auroras [45]. This debate remains unresolved, and the direct observation of a meteor shower on another planet remains an outstanding objective in planetary science.

### 2.1.3 Venus

Located at 0.7 AU from the Sun, Venus, with a diameter almost identical to Earth’s, experiences the highest meteoric influx among the inner planets that possess an atmosphere. The daily meteoric input is estimated at  $31.0 \pm 15.5$  t from the ZC. Predominantly, meteoroids originating from JFC contribute to 68% of this influx, with the remaining significant contribution coming from MBA orbits [38].

The atmosphere of Venus, predominantly consisting of 96.5% carbon dioxide, exerts a surface pressure about 92 times greater than Earth’s [2]. This denser atmosphere increases meteoroid ablation. Thus, meteoroids in Venus’s atmosphere achieve their maximum ablation — and consequently, their brightest observable magnitude — at higher altitudes and have a shorter lifespan than similar meteoroids in Earth’s atmosphere. Consequently, even smaller particles with diameters around  $200 \mu\text{m}$  can fully

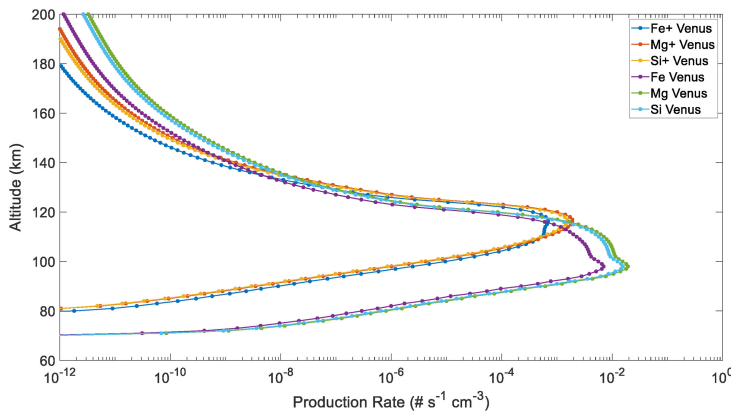


**Fig. 2–6: Neutral and ionic deposition rates of Mg, Fe, and Si on Venus [40].**

ablate, producing visible meteors [40].

Data derived from the Pioneer Venus and Venus Express missions indicate the presence of a metal layer within Venus's atmosphere, situated between altitudes of 115–120 km. This range aligns closely with the predicted meteoric ablation altitude, which spans from 110 to 120 km [40], as shown in Figure 2–6. Nevertheless, alternative ionization sources, including direct impact ionization by electrons or nocturnal proton precipitation, could potentially account for the properties of the lower ionospheric layer [27].

Though Venus's formative history paralleled Earth's — both planets underwent comet bombardments which introduced vast water quantities — the atmospheres of the two planets exhibit distinct water vapor concentrations. While Earth's atmosphere holds a water vapor percentage of 0.40%, Venus's atmosphere contains a mere 0.002% [2]. Discoveries made by the ESA's Venus Express spacecraft highlight the phenomenon of hydrogen and oxygen atoms being continually stripped from Venus due to the Sun's solar winds [2]. This suggests a potential meteoric source for the residual water detected in Venus's atmosphere.

#### 2.1.4 Titan

Titan, Saturn's largest moon situated at 9.5 AU, is distinctive among the satellites in the outer solar system for its substantial atmosphere. Titan's lower surface gravity, which is about a seventh of Earth's, results in a more expansive atmospheric layer. Its mesosphere, where the majority of meteoroid ablation occurs, spans from 300 km to 600 km. The atmosphere, predominantly nitrogen at 98.4%, has a surface pressure of 1.6 bar. Dust from Saturn's rings and volatile-rich cometary material from varied orbits (JFC, HFC, OCC) constitute the primary sources of meteoroids for Titan [46]. However, our understanding remains incomplete due to the reliance on data chiefly from the Voyager and Cassini missions.

Voyager 1 data indicates a composition of N<sub>2</sub> (1.4%) and CH<sub>4</sub> (0.2%) in Titan's stratosphere. Trace amounts of CO (60 ppm) and CO<sub>2</sub> (1.5 ppm) were also identified. The ablation of oxygen-bearing icy micrometeorites could introduce oxygen into Titan, with ablation altitudes for these molecules estimated between 600 km and 800 km [47].

Oxygen plays a pivotal role in astrobiology, particularly in the synthesis of amino acids and essential life-evolving chemical compounds [47]. Thermochemical simulations of N<sub>2</sub>/CH<sub>4</sub> atmospheres indicate the production of molecules like HCN, C<sub>2</sub>H<sub>2</sub>, C<sub>2</sub>H<sub>4</sub>, and H<sub>2</sub> from meteoroid material, especially at altitudes ranging from 200 km to 500 km [46].

Besides oxygen-bearing materials, meteoric ablation also introduces metallic atoms and ions into Titan's upper atmosphere, visualized in Figure 2–7. Na<sup>+</sup> and Fe<sup>+</sup> ions, which don't readily react with N<sub>2</sub> and CH<sub>4</sub>, could settle between altitudes of 650 km to 700 km, forming a metallic-ion layer [27, 48]. Cassini's radio occultation observations discovered a similar stable layer between 500 km and 700 km [49].

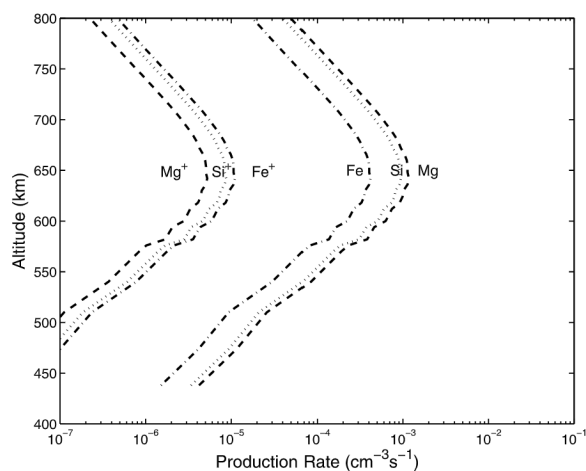


**Fig. 2–7: Neutral and ionic deposition rates of Mg, Fe, and Si on Titan [27].**

In the altitude range of 480 km to 600 km, conditions above Titan parallel those in Earth's polar mesosphere, where noctilucent clouds form around meteoroid particles due to water freezing. Water vapor detected in this region of Titan's atmosphere likely has meteoric origins [50]. Notably, despite recording various cloud patterns, Cassini did not detect any noctilucent clouds during its observations.

With the forthcoming Dragonfly mission, the mysteries shrouding Titan are anticipated to unfold, ushering in more comprehensive insights into this intriguing moon in the far reaches of our solar system.

### 3 Meteoroid Ablation Models

Meteor phenomena have been studied since the dawn of modern science. In 1798, two German students, Brandes and Benzenberg, employed simultaneous observations from separate locations to determine the altitude and speed of meteors. Their findings paved the way for the discipline, with their techniques serving as a basis for contemporary observations [21].

The journey of understanding meteoric events and their underlying physics saw significant contributions from researchers like Schiaparelli in the late 19th century and later by Kleiber, who proposed an essential equation related to meteoroid deceleration [51]:

$$\frac{dv}{dt} = -\frac{\Gamma S \rho_a v^2}{m} \quad (3-1)$$

Here,  $m$  denotes the mass,  $v$  the velocity,  $S$  the cross-sectional area,  $\rho_a$  the air density, and  $\Gamma = \frac{c_D}{2}$  is the drag coefficient.

As the 20th century ushered in technological advancements, observing techniques matured, enabling a frame-by-frame analysis of meteors. This, in turn, spurred the development of intricate models that delved into meteor-atmosphere interactions.

Central to understanding meteor phenomena is the concept of ablation, a complex interaction involving several physical processes. As meteoroids traverse the atmosphere, they undergo stresses leading to evaporation from air friction. Simultaneously, variations in atmospheric temperature and pressure can cause these bodies to fragment. Such interactions produce the phenomenon observed as meteors, composed of a prominent head, a trailing wake, and a lingering train or column. The balance between the thermal energy received from air molecules and the meteoroid's response mechanisms like radiative loss, melting, and vaporization play a crucial role [52].

The equation below captures this energy balance:

$$\pi R^2 \Lambda \frac{\rho_a v^3}{2} = 4\pi R^2 \epsilon \sigma_b (T_s^4 - T_0^4) + \frac{4}{3}\pi R^3 \rho_m c \frac{dT_s}{dt} - Q \frac{dm}{dt} \quad (3-2)$$

In Eq. (3-2), the term  $\pi R^2 \Lambda \frac{\rho_a v^3}{2}$  represents the energy flux absorbed by the meteoroid due to impacting air molecules. This energy is allocated among three primary processes: thermal radiation cooling, internal heating of the meteoroid, and ablation. The coefficient  $\Lambda$  signifies the heat transfer efficiency, dictating the proportion of the incoming energy flux that is absorbed by the meteoroid's surface. On the equation's right-hand side: the term  $4\pi R^2 \epsilon \sigma_b (T_s^4 - T_0^4)$  delineates the energy lost through radiation. Here,  $\epsilon$  stands for the emissivity coefficient,  $\sigma_b$  is the Stefan-Boltzmann constant, while  $T_s$  and  $T_0$  depict the temperatures of the meteoroid's surface and surrounding atmospheric environment, respectively. The subsequent term,  $\frac{4}{3}\pi R^3 \rho_m c \frac{dT_s}{dt}$ , pertains to



the energy requisite for raising the meteoroid's temperature. Within this term,  $c$  represents the bulk-specific heat and  $\rho_m$  denotes the meteoroid's density. The final term,  $Q \frac{dm}{dt}$ , characterizes the energy expended during the meteoroid's mass transfer into its gaseous phase. The variable  $Q$  encompasses the total energy necessary for both the melting and vaporization of the meteoroid material [8].

Further, the meteor's luminosity can be described by:

$$I = -\tau \frac{dE_k}{dt} = -\tau \left( \frac{v^2}{2} \frac{dm}{dt} + mv \frac{dv}{dt} \right) \quad (3-3)$$

In Eq. (3-3),  $I$  stands for the radiation's intensity,  $E_k$  for the meteoroid's kinetic energy, and  $\tau$  is the luminosity efficiency. The brightness of a meteor is inherently linked to various factors, including size, mass, entry velocity, flight altitude, and inherent meteoroid properties [8].

With this foundation, this chapter delves into the meteoroid ablation models developed over the last century to capture and explain these intricate phenomena.

### 3.1 Meteoroid single-body ablation models

The first ablation model was introduced by Lindemann in 1927 to primarily determine mesospheric density and temperature using eye observations of meteors. This model posited that meteoroids lost mass solely through material evaporation, treating the object as a single solid body. Although Lindemann's model provided valuable insights, its inconsistent results were primarily attributed to the imprecise nature of eye observations of meteor velocity [53].

To optimize a model, accurate data is indispensable. Therefore, the adoption of Lindemann's model awaited technological advancements. After World War II, James G. Baker engineered the first Schmidt camera tailored for meteor photography. This camera, equipped with a mechanical chopper, facilitated frame-by-frame analysis of a meteor's trajectory. It gained popularity across the US and Canada, becoming the benchmark for meteor observation [21].

Empowered by this technology, the meteorological community refined Lindemann's model, dubbing it the "single-body ablation model." This iteration posits that small meteoroids begin to shed parts upon atmospheric entry due to sputtering. As these meteoroids descend, they reach an intensive evaporation height where most of their mass vaporizes in milliseconds [52]. Below this altitude, factors like heat conduction and thermal radiation become negligible, making the heat equation predominantly governed by meteoroid material evaporation.

$$\frac{dm}{dt} = -\Lambda \frac{\pi R^2 \rho_a v^3}{2Q} \quad (3-4)$$

By transforming the differential equations governing meteoroid movement and ablation, one can establish relationships between mass change, velocity, and the ablation

coefficient  $\sigma$ , and other meteoroid characteristics encapsulated in  $K$  [52].

$$\frac{dm}{dt} = -K\sigma m^{2/3} \rho_a v^3 \quad (3-5)$$

The ablation coefficient  $\sigma$  and the density shape coefficient  $K$  are in general constants in the equation.

$$\sigma = \frac{\Lambda}{2Q\Gamma} \quad K = \Gamma A \rho_m^{-2/3} \quad (3-6)$$

In  $K$ , the shape factor  $A = S(\rho_m/m)^{2/3}$  allows the model to account for changes in shape during the ablation process. A sphere, for instance, has a value of  $A = 1.2$ , as shown in Figure 3–1.

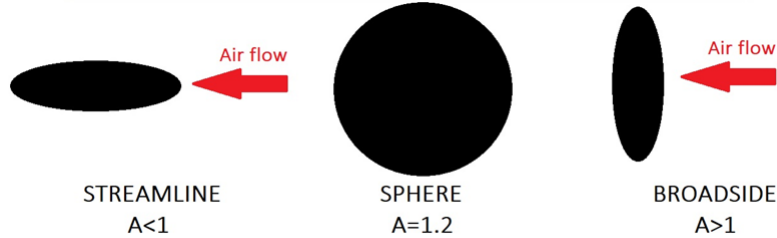


**Fig. 3–1: Shape factor visualization for various forms.**

Interestingly, the very camera that facilitated the model's adoption was later employed to identify its limitations. In mid-20th century, it was well known that some meteor trail lengths were anomalously shorter than those predicted by the single-body ablation model. In 1955, Jacchia deduced that smaller meteoroids could fragment, an observation challenging the single-body ablation model's assumptions [54].

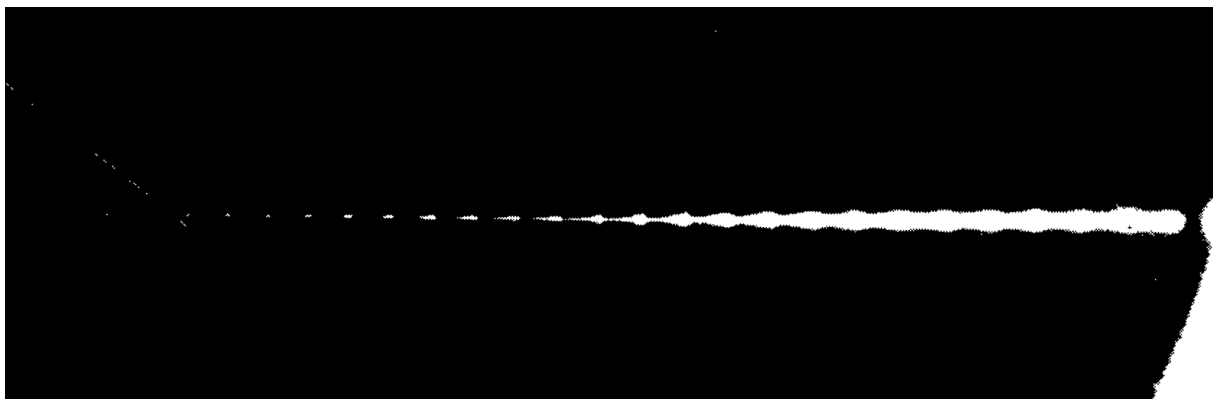


**Fig. 3–2: Meteor showing terminal blending [55].**

Schmidt camera equipped with a mechanical chopper, segmented the meteor's light during each frame, resulting in an image with individual points capturing the meteor's



successive positions, as shown in Figure 3–2. Meteoroids were predominantly perceived as solid entities that radiated light while traversing the frames as a point source [55]. In New Mexico, Jacchia defined the material spanning the gaps between frames at the end of the trail, so-called “terminal blending” and the notable decline in velocity were undeniable evidence of meteoroid fragmentation [54].

Despite its limitations, due to its simplicity and minimal parameter tuning, this model remains popular. However, it’s recognized that neglecting fragmentation can yield inflated ablation coefficients  $\sigma$  and density  $\rho_m$  underestimations [8].

### 3.2 Dust-ball Fragmentation Models

The concept of meteoroids as conglomerates of refractory grains held together by a weaker “glue” material was first introduced by Opik in 1958, who termed this configuration a “dustball”. The notion challenged the prevailing view of meteoroids as solid, cohesive entities, suggesting instead that they possess a more intricate internal structure [52].

In 1975, Hawkes and Jones further developed this idea, presenting the “dust-ball fragmentation model.” According to this model, meteoroids consist of solid grains with significantly higher boiling points than the binding “glue” material, typically around 1300 K. Upon reaching the boiling point of the “glue”, the grains are released, a process quantified by the energy of disintegration,  $X$ :

$$X = \frac{c\Delta T + fL}{(1-f)^{1/3}} \quad (3-7)$$

Where  $c$  represents the heat capacity,  $\Delta T$  is the temperature difference between the initial state and the boiling point of the glue,  $L$  is the latent heat of vaporization for the binding material, and  $f$  is the fraction of the meteoroid mass attributed to the binding material.

Such a model effectively describes the flake-like meteoroids observed through Schmidt cameras. These meteoroids undergo disintegration before becoming visually discernible, leading to detached grains that ablate independently. Notably, these meteoroids exhibit a unique light curve peak at the onset, corresponding to the moment when all fragments reach the point of intense ablation, and then quickly diminish [56].

Many of these small, flake-like meteoroids, believed to be cometary ash, are held together by weak Van der Waals forces, as shown in Figure 3–3. In-situ cometary data suggest that the constituent particles of these meteoroids are likely larger than  $10^{-10}$  kg, a finding consistent with planetary formation models [57]. Contemporary observations reveal that nearly 90% of faint meteors captured by high-resolution video cameras display some fragmentation behavior [58]. Larger meteoroids, however, often exhibit minimal fragmentation due to their predominantly solid nature, resulting in simultaneous ablation and grain detachment [56].

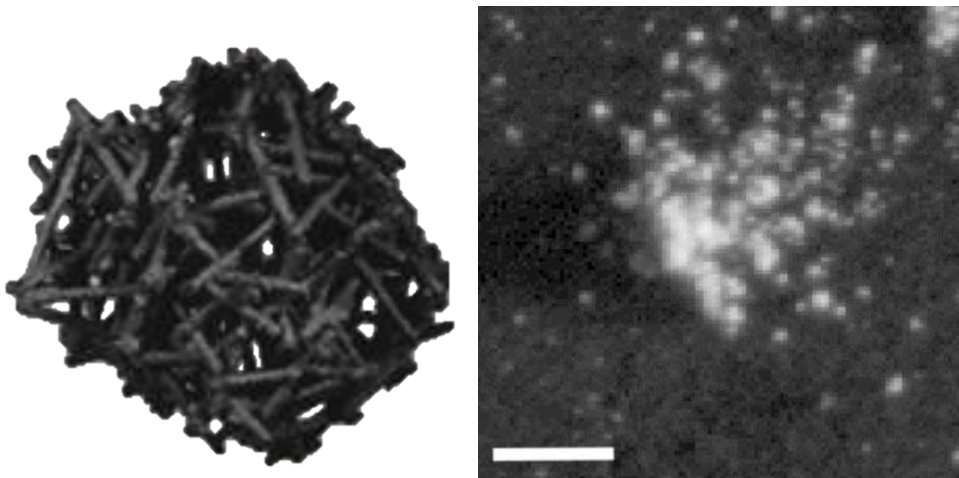


**Fig. 3-3:** Right: Theoretical depiction of a flake-like meteoroid within the dustball model. Left: Actual cometary dust from Comet 67/P retrieved by the Rosetta mission. Scale bar represents  $200 \mu\text{m}$  [57].

The dust-ball fragmentation model has been pivotal in simulating the rapid dispersal of grains, culminating in luminous flares characterized by a steep onset. This characteristic makes it particularly challenging to model in certain scenarios. Nevertheless, the foundational dust-ball structure has inspired the development of numerous models, each aiming to accurately replicate the vast range of observed meteor phenomena.

### 3.2.1 Thermal Disruption Model

Campbell-Brown and Koshny, in 2004, extended the foundation set by the dustball fragmentation model, proposing a model which accounts for fragmentation due to the sustained release of particles from a meteoroid's rapidly heated exterior [59]. As a meteoroid enters an atmosphere, its surface encounters intense heat over a brief time span, primarily warming its outer layer.

In their model, the temperature increase within a shell of thickness  $x_0$  is assumed to be uniform, while the meteoroid's inner core remains relatively cool. The depth  $x_0$  represents the region where the temperature drops to  $1/e$  of the surface value:

$$x_0 = \sqrt{\frac{\lambda_c}{\rho_m c v_\infty} \frac{H^*}{\cos(z)}} \quad (3-8)$$

Where  $\lambda_c$  denotes the thermal conductivity of the meteoroid,  $H^*$  is the atmospheric scale height,  $v_\infty$  is the meteoroid's velocity outside the atmosphere and  $z$  is the zenith angle.

Depending on the mass of the heated layer, different fragment distributions can emerge. For instance, with a Gaussian distribution of fragments, a late-peaking light curve is observed, which is shorter compared to that of a cohesive body. Adjusting the average grain size can further modulate the duration and peak height of the curve [59].



However, the model does present uncertainties, primarily tied to the coefficient of luminous intensity and the heat transfer coefficient. Misestimations in these parameters can lead to inaccuracies in the calculated grain sizes. Moreover, using this model a significant number of fragments are predominantly released early on. This makes achieving precise control over the wake challenging, so fitting the model can be particularly difficult towards the end of observations [59].

### 3.2.2 Erosion Fragmentation Model

In 2007, Borovička, Spurný, and Koten introduced the Erosion Fragmentation Model, devised specifically for simulating cometary meteoroids [60]. Building upon the dust-ball model's foundation, this semi-empirical approach incorporates a quasi-continuous fragmentation mechanism termed as "erosion". The core objective of this model is to identify fragmentation instances, which are typically discernible from the light curve. Fragmentation altitudes, denoted by  $h_f$ , are derived manually, utilizing a trial-and-error method that best fits the observed decelerations and light curves.

The erosion rate in the model is characterized by the erosion coefficient,  $\eta_{er}$ , which functions similarly to the ablation coefficient,  $\sigma$ :

$$\frac{dm}{dt} = -K(\sigma + \eta_{er})m^{2/3}\rho_a v^3 \quad (3-9)$$

This model envisions the creation of numerous fragments within a specified mass range, determined by the upper and lower mass limits,  $m_u$  and  $m_l$ , and the mass distribution index,  $s$ . The index outlines the grain masses released, conforming to a power-law mass distribution expressed as  $n(m) \approx m^{-s}$ . Depending on grain density, individual meteoroids of mm-size encompass anywhere from tens of thousands to close to a million grains. Once detached, all fragments undergo ablation as singular entities, maintaining uniform  $K$  and  $\sigma$  values. Fragmentation generally commences once the meteoroid's surface accrues an energy of  $10^6$  J/m<sup>2</sup>. The model's capability encompasses considering multiple fragmentation events, with the generated luminosity scaled by the number of fragments and the principal fragments that release them [60].

Conventional photographic observations primarily yield dynamic data for only the most massive leading fragment. However, leveraging high-resolution video recordings, individual fragment tracking becomes feasible, enhancing the granularity of fragmentation modeling using the erosion model [60].

A distinguishing aspect of the Erosion Fragmentation Model is its inherent flexibility, attributed to its extensive set of tunable variables. This enables fine-tuning of fragment releases at any altitude, a critical feature for achieving precise wake control. Unlike other models where fragmentation is contingent upon specific energy (as in the dustball model) or temperature benchmarks (as seen in the thermal disruption model), this model facilitates fragmentation at determined altitudes, achieved by manual data fitting. Currently, the Western Meteor Physics Group (WMPG) at Western University employs this versatile model in their research.

## 4 PhD Research Project

This research thesis aims to devise a statistical meteoroid ablation and fragmentation model grounded in erosion principles, underpinned by optical data from known meteor events. These events were recorded by the CAMO and EMCCD cameras stationed at Elginfield and Tavistock. The model's eventual ambition is to characterize Earth's faint meteor environment statistically and then extrapolate this understanding to various planetary atmospheres.

### 4.1 Research Focus

Meteoroid material predominantly originates from JFC or MBA orbits emanating from the Helion/Anti-Helion region in the sun-centric frame of reference, as detailed in chapter 1. These meteoroids impacting Earth's atmosphere, exhibit considerably low velocities, as depicted in figure 4–1. Such reduced speeds imply that primarily the heavier meteoroids (around  $10^{-3}$  g) translate to observable meteors, most likely within the magnitude range of 9 to -1.

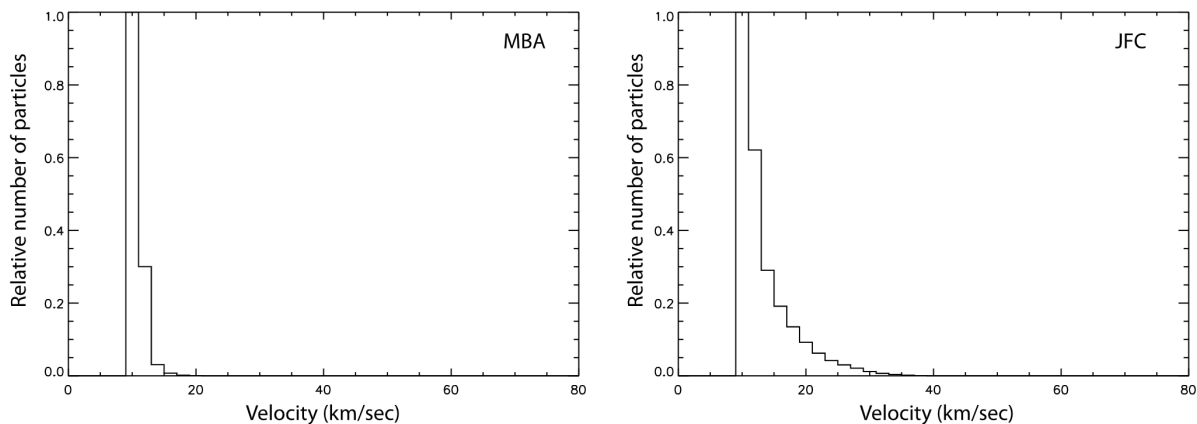


**Fig. 4–1: Velocity distributions of meteoroids from JFC and MBA at 1 AU [61].**

This research is particularly attuned to sporadic meteoroids, both sub-mm and cm in size, moving at speeds below 20 km/s. The fragmenting meteoroids chosen for analysis will have their attributes inferred via the erosion model, as elaborated in chapter 3. The data curated from this select set of events will demarcate the distribution spectrum for ablation parameters, erosion energy, and the deposition patterns of both smaller and larger meteor grains—essential for crafting the statistical model. Consequently, this dataset promises a deeper insight into the physical and structural aspects of the more substantial meteoroids in the zodiacal cloud, enhancing our grasp of the solar system's meteoroid environment.

## 4.2 Research Instrumentation

As previously discussed in chapter 2, both radar and optical tools offer insights into faint meteors' fragmentation patterns.

Radar observations primarily capture the echo intensity resulting from reflections off two or more distinct fragments, each separated by a substantial portion of the radar's wavelength. These observations, due to their high sensitivity, can identify even the faintest of meteors. However, this sensitivity also introduces susceptibility to noise. The recorded echoes can vary due to instrumental effects, constructive and destructive interference patterns between fragments, or fluctuations in the ablation rate [62].

In contrast, optical observations, while less sensitive than radar, boast a higher reliability quotient. Fragmentation becomes discernible when the fragment separation surpasses the system's resolution threshold. Standard cameras for faint meteors typically showcase fragmentation as a luminous wake. For more granular fragment resolution, telescopic observations can be employed, provided they can track the meteor's trajectory. Otherwise, the meteor's representation could blur, spanning several degrees in the image [11].

For this research endeavor, the focal point will be the optical observations derived from meteoroid events, harnessing data from both Canadian Automated Meteor Observatory (CAMO) and Electron Multiplying Charge-Coupled Device (EMCCD).

### 4.2.1 CAMO: Telescopic Observation System

The CAMO offers a unique advantage in meteor observation. Compared to conventional optical meteor cameras, the CAMO can capture faint meteor fragments at an enhanced resolution. This superior resolution aids in detailing the fragmentation behavior of meteoroids across a myriad of observations [63].

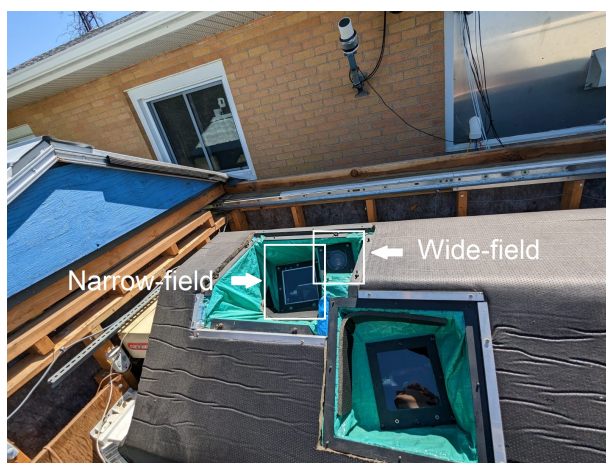


**Fig. 4–2:** Wide-field and Narrow-field CAMO cameras shown in white at Elginfield observatory.

The CAMO system integrates wide-field CCD cameras, boasting a 30-degree field of view, that can detect meteors of up to 4 magnitude. Once a meteor is detected, the

system employs mirrors and a high-resolution, narrow-field CCD camera (with approximately a 1.5-degree field of view) affixed to an f/11 telescope to track the meteor. This narrow-field camera can resolve details as minuscule as 4 meters for magnitudes up to -1 [63]. As depicted in figure 4–2, the design architecture is unique and stands as the sole operational telescopic tracking system for meteor observations [11].

The granularity offered by the CAMO is reminiscent of the sensitivity radar measurements offer but with a reduced noise profile. For this research, the CAMO will be indispensable in precisely characterizing meteoroid fragmentation.

#### 4.2.2 EMCCD: Enhanced Meteor Imaging

While CCD cameras deliver the requisite frames per second (frames per second (FPS)) for meteor observation, their short exposure durations can be limiting in capturing extremely faint meteors. EMCCD cameras offer a workaround, delivering superior effective read noise at high gains even with short exposures, outperforming standard CCD cameras [64].

The Western Meteor Physics Group (WMPG) has deployed four EMCCD medium-field cameras across their main sites at Elginfield and Tavistock. The EMCCD Nüvü HNÜ1024 cameras of WMPG can discern faint meteors with magnitudes up to 9. Typically, these cameras use 2x2 binning to achieve 32 fps. As illustrated in figure 4–3, one camera pair is angled at an elevation of roughly 70 degrees, capturing meteors above 90 km. The other set, angled at approximately 40 degrees, captures meteors ranging from 70 km to 120 km in altitude [64].



**Fig. 4–3: Two EMCCD cameras at Elginfield observatory positioned at 70 deg and 40 deg elevations.**

The data captured by the EMCCD will be instrumental in evaluating Earth's meteor environment. Despite its coarser fragmentation resolution, the EMCCD remains valuable in shedding light on the initial and concluding phases of meteor events. This data will complement the high-resolution observations made by the CAMO, especially since the latter cannot discern extremely faint magnitudes.

## 4.3 Research Overview

This research aims to deepen our understanding of faint meteoroids and their behavior in Earth's atmosphere, providing a more refined perspective on meteoroid physical characteristics and their potential implications for satellite safety and planetary atmosphere meteoroid interaction.

### 4.3.1 Meteor Characteristics and Selection Criteria

Faint meteoroids observable are bound by specific constraints. The constraints include the velocity of the sporadic population, set at 20 km/s, and the maximum magnitude resolvable by CAMO, which is 4 mag. Our study's meteoroids represent a specific subset of the entire meteoroid flux impacting Earth, visualized in figure 4–4.

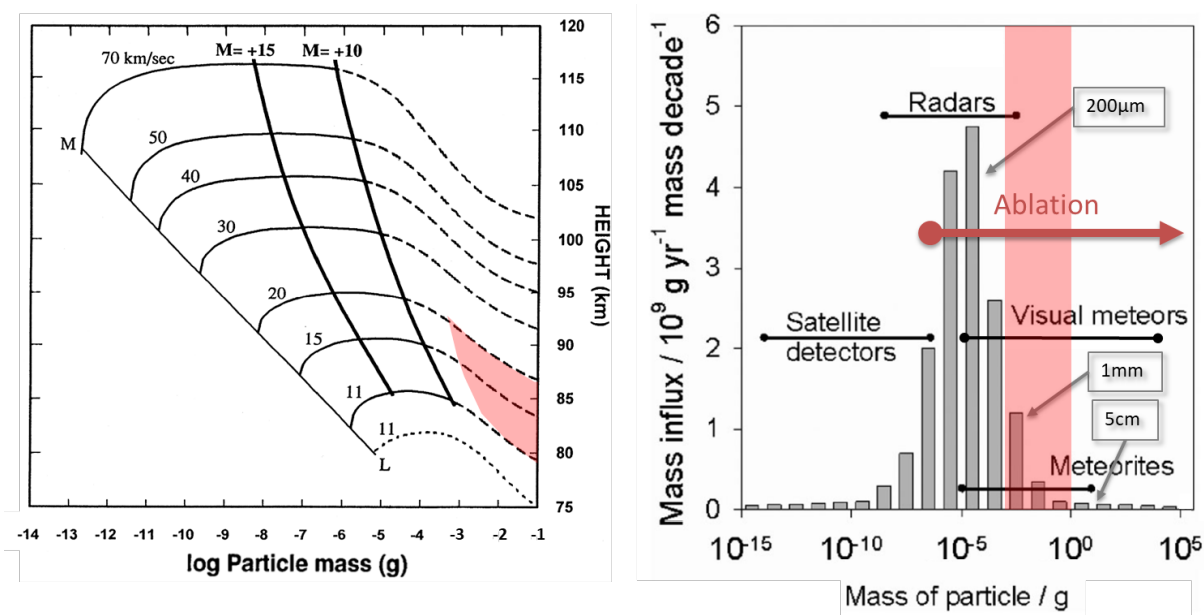


**Fig. 4–4:** On the left, we observe the initiation heights for stony particles entering at 45 deg, plotted as a function of their mass, velocity, and absolute magnitude [5]. On the right, the flux is mapped considering the observable meteoroid range [14]. The regions earmarked in red delineate our study's focus.

Our analysis is grounded in the examination of a dozen of meteoroid events recorded from 2018 to 2023. These events, characterized by their specific observable features, have been meticulously tracked by CAMO and also captured by EMCCD cameras. These meteoroids predominantly stem from the anthelion region, the sole source that can be clearly imaged using optical cameras.

### 4.3.2 Data Analysis and Model Development

Utilizing the METAL and MIRFIT tools from WMPG, we intend to process the recorded data, as shown in Figure 4–5. The subsequent analysis with the MetSim from the wmpf python library will enable the extraction of meteoroid erosion parameters. Through a Monte Carlo method, we will sample across the parameter ranges to produce a

synthetic fragmentation-based model of meteor behavior. By adapting the MetSim model, developed by WMPG, we aim to design a Bayesian Monte Carlo model that integrates statistical fragmentation characteristics.

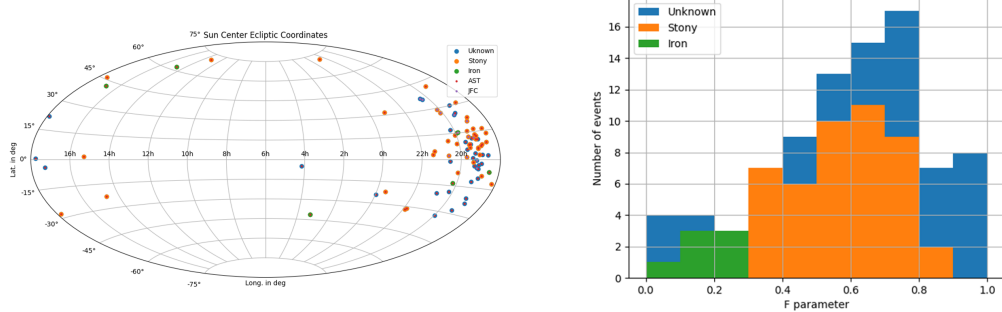


**Fig. 4–5:** The selected meteoroid events, characterized by their known properties, plotted in a concentric reference frame [61].

The final outcome will be a scientifically robust fragmentation model, providing insights into the attributes of sporadic meteoroids, their implications for satellite risk assessment, and their potential influence on NASA's MEM. Central to NASA's endeavors, the MEM furnishes invaluable information regarding meteoroid environments at different altitudes around Earth and other celestial bodies. Such understanding is pivotal to fortifying both manned and unmanned space missions against potential meteoroid threats.

#### 4.3.3 Meteoroid Physical Characteristics Range

For enhanced accuracy of our Monte Carlo simulation model, Principal Components Analysis (PCA) [65] will offer a nuanced uncertainty range for the fitted meteor events.

Traditional ablation models are typically employed to derive physical properties of meteoroids from singular events [51]. The aim has been to establish automated methodologies for characterizing these properties, as discussed in recent works [66]. However, due to the vast variability and complexity of meteoroid physical parameters, deriving unique and automated attributes for individual meteor events remains a challenge.

In response, our approach leverages Principal Components Analysis (PCA) [65] on an extensive dataset of faint meteors detected using EMCCD and a synthetic meteor dataset generated based on the erosion model, detailed in section 3. By correlating PCA components from real meteor observations with those from synthetic datasets, we aim to deduce a range of possible physical attributes of the actual meteors observed, as shown in Figure 4–6. This strategy provides a broader spectrum of potential values representing possible physical characteristics for a group of events or a single meteor, useful for our Monte Carlo simulation model.

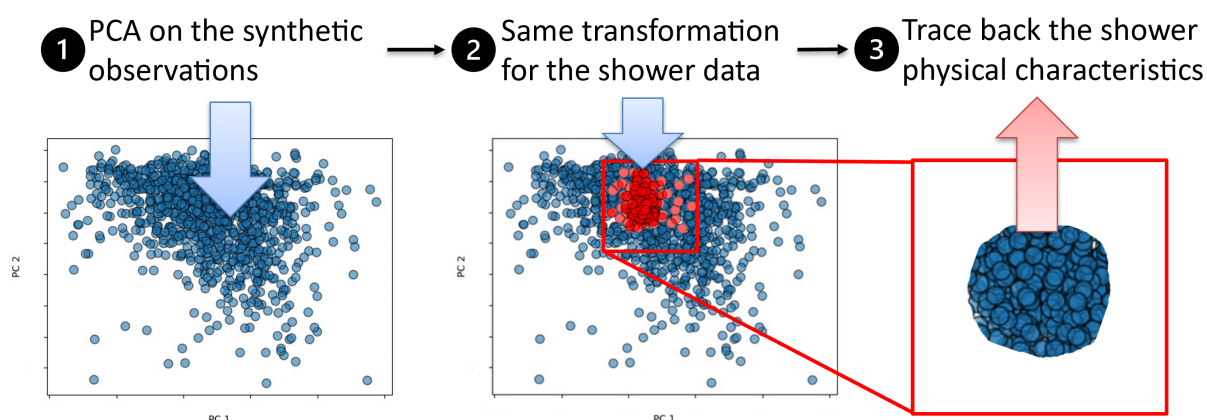


**Fig. 4–6: Processing of a group of meteor events with PCA.**

#### 4.3.4 Interplanetary Application

A significant limitation in understanding meteors on other planets is the current reliance on single-body ablation models due to the challenges of instrumentation and empirical data scarcity.

Our research will bridge this gap by adapting our fragmentation Monte Carlo model to simulate meteor behavior in different planetary atmospheres like Venus, Mars, and Titan. This novel approach will lay the foundation for future interplanetary missions, offering guidance on instrument design and objectives.

### 4.4 Research Work Structure

The PhD project, set to commence in January 2023, spans a duration of 4 years. The tasks are methodically segmented into 5 primary Work Packedges (WP), each informing and refining subsequent phases, as outlined in table 4–1. The stages include:

- WP 0: Compulsory PhD coursework.
- WP 1: Application of Principal Components Analysis to meteor data.
- WP 2: Development of a Monte Carlo statistical fragmentation model.
- WP 3: Extension of the Monte Carlo model to different planetary atmospheres.
- WP 4: Dissertation composition.

WP 0 encompasses the essential courses and comprehensive modules integral to the Astronomy PhD and the Collaborative Specialization in Planetary Science & Exploration at Western University.

WP 1 entails the necessary procedures for publishing an inaugural paper on employing the Principal Components Analysis to derive statistically erosion parameters for observed meteor populations and single events. This foundational work will steer the genesis of the statistical Monte Carlo model delineated in WP 2.

**Tab. 4–1: Strategic division of tasks for the PhD project, organized by semester. The stripe pattern denotes tasks that may require adjustment or might extend across multiple semesters.**

WP	Titles		2023 W	2023 S	2023 A	2024 W	2024 S	2024 A	2025 W	2025 S	2025 A	2026 W	2026 S	2026 A
WP.0.1	0.5 HCE; ASTR exam 1													
WP.0.2	0.5 HCE; ASTR/PLANETSC exam 2													
WP.0.3	0.5 HCE; PLANETSC exam 3													
WP.0.4	0.5 HCE; Planet Scien. Short C.													
WP.0.5	Graduate Seminar ASTR													
WP.0.6	Graduate Seminar PLANETSC													
WP.0.7	1st Compr. Intr. Modern Astro.													
WP.0.8	2nd Compr. Lit. Review													
WP.1.1	Python code PCA													
WP.1.2	Apply PCA to different shower													
WP.1.3	Metsim manual reduction													
WP.1.4	Apply on CAMO													
WP.1.5	1st paper writing													
WP.1.6	1st paper review													
WP.2.1	METAL/MIRFIT/linux setup													
WP.2.2	METAL/MIRFIT Reductions													
WP.2.3	Metsim reduction and data													
WP.2.4	Montecarlo simulations													
WP.2.5	Earth EMCCD test													
WP.2.6	2st paper writing													
WP.2.7	2st paper review													
WP.3.1	Montecarlo simulations planets													
WP.3.2	Apply on Mars													
WP.3.3	Apply on Venus													
WP.3.4	Apply on Titan													
WP.3.5	Satellite/camera mission													
WP.3.6	3st paper writing													
WP.4.1	Tthesis writing													



It is crucial that all tasks under WP 2, excluding manuscript drafting and peer review, conclude by 2025's end. This is because the models crafted by WMPG are anticipated to integrate into the fourth release of MEM that year.

WP 3 is theoretical in nature, driven by the dearth of meteor data from diverse planets, necessitating reliance on existing theoretical frameworks and sparse in-situ missions. While the timeline might be extended, the entirety of this work is aligned with the four-year PhD timeline.

Lastly, WP 4 encapsulates the research journey, culminating in the dissertation's drafting, expected to conclude by 2026 as stipulated by Western University.

## 4.5 Research Objectives

This study endeavors to offer an enriched understanding of meteoroids, their behavior, and their broader implications, both for Earth and other planets. By integrating a statistical approach with the fragmentation model and applying it to different planetary atmospheres. These findings will not only further academic knowledge but also have tangible applications, particularly in satellite safety and future interplanetary mission designs.

## Bibliography

- [1] A. Egal, "Forecasting meteor showers: A review," *Planetary and Space Science*, vol. 185, p. 104895, 2020.
- [2] J. Lissauer and I. de Pater, *Fundamental Planetary Science: Physics, Chemistry and Habitability*. Cambridge University Press, 2019.
- [3] B. Gladman, L. Dones, H. F. Levison, and J. A. Burns, "Impact seeding and re-seeding in the inner solar system," *Astrobiology*, vol. 5, no. 4, pp. 483–496, 2005.
- [4] S. A. Nelson, "Meteorites, impacts, and mass extinction," [https://www2.tulane.edu/~sanelson/Natural\\_Disasters/impacts.htm](https://www2.tulane.edu/~sanelson/Natural_Disasters/impacts.htm), 2018, viewed 14-July-2023.
- [5] Z. Ceplecha, J. Borovička, W. G. Elford, D. O. ReVelle, R. L. Hawkes, V. Porubčan, and M. Šimek, "Meteor phenomena and bodies," *Space Science Reviews*, vol. 84, no. 3, pp. 327–471, 1998.
- [6] IAU, "Definitions of terms in meteor astronomy," [https://www.iau.org/static/science/scientific\\_bodies/commissions/f1/meteordefinitions\\_approved.pdf](https://www.iau.org/static/science/scientific_bodies/commissions/f1/meteordefinitions_approved.pdf), 2017, viewed 7-July-2023.
- [7] G. J. Flynn, G. J. Consolmagno, P. Brown, and R. J. Macke, "Physical properties of the stone meteorites: Implications for the properties of their parent bodies," *Geochemistry*, vol. 78, no. 3, pp. 269–298, 2018.
- [8] O. Popova, J. Borovicka, and M. Campbell-Brown, "Modelling the entry of meteoroids," *Meteoroids: Sources of Meteors on Earth and Beyond*, vol. 25, no. 9, 2019.
- [9] A. V. Moorhead and G. C. Marshall, "Nasa meteoroid engineering model (mem) version 3," 2020. [Online]. Available: <http://www.sti.nasa.gov>
- [10] Soja, R. H., Grün, E., Strub, P., Sommer, M., Millinger, M., Vaubaillon, J., Alius, W., Camodeca, G., Hein, F., Laskar, J., Gastineau, M., Fienga, A., Schwarzkopf, G. J., Herzog, J., Gutsche, K., Skuppin, N., and Srama, R., "Imem2: a meteoroid environment model for the inner solar system," *A&A*, vol. 628, p. A109, 2019. [Online]. Available: <https://doi.org/10.1051/0004-6361/201834892>
- [11] J. Borovička, R. J. Macke, M. D. Campbell-Brown, A.-C. Levasseur-Regourd, F. J. Rietmeijer, and T. Kohout, "Physical and chemical properties of meteoroids," *Meteoroids: Sources of meteors on earth and beyond*, p. 37, 2019.
- [12] E. J. Opik, *Physics of Meteor Flight in the Atmosphere*, 1958.
- [13] J. M. Trigo-Rodríguez, *The flux of meteoroids over time: meteor emission spectroscopy and the delivery of volatiles and chondritic materials to Earth*. IOP Publishing, 3 2019.
- [14] ——, *The flux of meteoroids over time: meteor emission spectroscopy and the delivery of volatiles and chondritic materials to Earth*. IOP Publishing, 3 2019.



## Bibliography

- [15] T. Mills, P. Brown, M. Mazur, D. Vida, P. S. Gural, and A. V. Moorhead, "Iron rain: measuring the occurrence rate and origin of small iron meteoroids at earth," *Monthly Notices of the Royal Astronomical Society*, vol. 508, no. 3, pp. 3684–3696, 2021.
- [16] V. Vojáček, J. Borovička, P. Koten, P. Spurný, and R. Štork, "Properties of small meteoroids studied by meteor video observations," *Astronomy and Astrophysics*, vol. 621, pp. 1–21, 2019.
- [17] D. Nesvorný, P. Jenniskens, H. F. Levison, W. F. Bottke, D. Vokrouhlický, and M. Gounelle, "Cometary origin of the zodiacal cloud and carbonaceous micrometeorites. implications for hot debris disks," *The Astrophysical Journal*, vol. 713, no. 2, p. 816, 2010.
- [18] V. A. Bronshten, *Physics of meteoric phenomena*. Springer Science & Business Media, 1983, vol. 22.
- [19] H. Levison, "Comet taxonomy," T. Rettig and J. Hahn, Eds. Astronomical Society of the Pacific, 1996, pp. 173–191.
- [20] J. Jones and P. Brown, "Sporadic meteor radiant distributions: orbital survey results," *Monthly Notices of the Royal Astronomical Society*, vol. 265, no. 3, pp. 524–532, 1993.
- [21] D. McKinley, *Meteor Science and Engineering*. McGraw-Hill, 1961.
- [22] J. C. Solem, "Cometary breakup calculations based on a gravitationally-bound agglomeration model: the density and size of Shoemaker-Levy 9.", vol. 302, p. 596, Oct. 1995.
- [23] A. A. Christou, "Annual meteor showers at Venus and Mars: lessons from the Earth," *Monthly Notices of the Royal Astronomical Society*, vol. 402, no. 4, pp. 2759–2770, 03 2010. [Online]. Available: <https://doi.org/10.1111/j.1365-2966.2009.16097.x>
- [24] E. Grün, H. Zook, H. Fechtig, and R. Giese, "Collisional balance of the meteoritic complex," *Icarus*, vol. 62, no. 2, pp. 244–272, 1985. [Online]. Available: <https://www.sciencedirect.com/science/article/pii/0019103585901216>
- [25] JPL, "Dust disks," <https://www.jpl.nasa.gov/infographics/dust-disks>, 2012, viewed 20-July-2023.
- [26] J. D. Carrillo-Sánchez, J. C. Gómez-Martín, D. L. Bones, D. Nesvorný, P. Pokorný, M. Benna, G. J. Flynn, and J. M. Plane, "Cosmic dust fluxes in the atmospheres of earth, mars, and venus," *Icarus*, vol. 335, 1 2020.
- [27] J. G. Molina-Cuberos, J. J. López-Moreno, and F. Arnold, "Meteoric layers in planetary atmospheres," *Space Science Reviews*, vol. 137, pp. 175–191, 6 2008.
- [28] S. E. Pratt., "Looking for lightning, finding fireballs," <https://earthobservatory.nasa.gov/images/149381/looking-for-lightning-finding-fireballs>, 2022, viewed 13-July-2023.

- [29] A. M. Society, "Fireball faqs," <https://www.amsmeteors.org/fireballs/faqs/>, 2022, viewed 20-October-2022.
- [30] P. Jenniskens, J. Albers, C. E. Tillier, S. F. Edgington, R. S. Longenbaugh, S. J. Goodman, S. D. Rudlosky, A. R. Hildebrand, L. Hanton, F. Ciceri *et al.*, "Detection of meteoroid impacts by the geostationary lightning mapper on the goes-16 satellite," *Meteoritics & Planetary Science*, vol. 53, no. 12, pp. 2445–2469, 2018.
- [31] NOAA, "Instruments: Geostationary lightning mapper (glm)," <https://www.goes-r.gov/spacesegment/glm.html>, viewed 17-July-2023.
- [32] G. Flynn, E. Murad, and I. Williams, "Meteors in the earth's atmosphere," 2002.
- [33] S. G. Love and D. E. Brownlee, "A direct measurement of the terrestrial mass accretion rate of cosmic dust," *Science*, vol. 262, pp. 550–553, 10 1993.
- [34] J. Plane, "Cosmic dust in the earth's atmosphere," *Chemical Society Reviews*, vol. 41, pp. 6507–6518, 9 2012.
- [35] J. M. Plane, "Atmospheric chemistry of meteoric metals," *Chemical Reviews*, vol. 103, pp. 4963–4984, 12 2003.
- [36] M. Rapp and G. E. Thomas, "Modeling the microphysics of mesospheric ice particles: Assessment of current capabilities and basic sensitivities," *Journal of Atmospheric and Solar-Terrestrial Physics*, vol. 68, no. 7, pp. 715–744, 2006. [Online]. Available: <https://www.sciencedirect.com/science/article/pii/S1364682605003007>
- [37] K. S. Johnson, "Iron supply and demand in the upper ocean: Is extraterrestrial dust a significant source of bioavailable iron?" *Global Biogeochemical Cycles*, vol. 15, no. 1, pp. 61–63, 2001. [Online]. Available: <https://agupubs.onlinelibrary.wiley.com/doi/abs/10.1029/2000GB001295>
- [38] J. D. Carrillo-Sánchez, J. C. Gómez-Martín, D. L. Bones, D. Nesvorný, P. Pokorný, M. Benna, G. Flynn, and J. Plane, "Cosmic dust fluxes in the atmospheres of earth, mars, and venus," *Icarus*, p. 113395, 8 2019. [Online]. Available: <https://doi.org/10.1016/j.icarus.2019.113395> <https://linkinghub.elsevier.com/retrieve/pii/S0019103519301824>
- [39] G. J. Flynn and D. S. McKay, "An assessment of the meteoritic contribution to the martian soil," *Journal of Geophysical Research*, vol. 95, 1990.
- [40] J. P. Pabari, S. N. Nambiar, Rashmi, and S. Jitarwal, "Metallic ion layers in planetary atmosphere: Boundary conditions and idp flux," *Planetary and Space Science*, vol. 226, 2 2023.
- [41] L. G. Adolfsson, B. Gustafson, and C. D. Murray, "The martian atmosphere as a meteoroid detector," *Icarus*, vol. 119, pp. 144–152, 1 1996.
- [42] J. Vaubaillon, F. Selsis, M. Lemmon, and J. Bell, "Identification of the first martian meteor," in *Proceedings of the International Meteor Conference, 24th IMC, Oostmalle, Belgium, 2005*, 2006, pp. 152–154.



## Bibliography

- [43] J.-E. Collaboration, J. Adams, S. Ahmad, J. N. Albert, D. Allard, L. Anchordoqui, V. Andreev, A. Anzalone, Y. Arai, K. Asano *et al.*, “Jem-euso: Meteor and nuclearite observations,” *Experimental Astronomy*, vol. 40, pp. 253–279, 2015.
- [44] V. L. Hartwick, O. B. Toon, and N. G. Heavens, “High-altitude water ice cloud formation on mars controlled by interplanetary dust particles,” *Nature Geoscience*, vol. 12, pp. 516–521, 7 2019.
- [45] J. D. Carrillo-Sánchez, D. Janches, J. M. Plane, P. Pokorný, M. Sarantos, M. M. Crismani, W. Feng, and D. R. Marsh, “A modeling study of the seasonal, latitudinal, and temporal distribution of the meteoroid mass input at mars: Constraining the deposition of meteoric ablated metals in the upper atmosphere,” *Planetary Science Journal*, vol. 3, p. 239, 2022. [Online]. Available: <http://dx.doi.org/10.3847/PSJ/ac8540>
- [46] E. E. Flowers and C. F. Chyba, “Shock synthesis of organic molecules by meteoroids in the atmosphere of titan,” *The Planetary Science Journal*, vol. 4, p. 127, 7 2023. [Online]. Available: <https://iopscience.iop.org/article/10.3847/PSJ/acdfc9>
- [47] E. C. . Sittler, A. Ali, J. F. Cooper, R. E. Hartle, R. E. Johnson‘, A. J. C. Johnson‘, and D. T. Young, “Heavy ion formation in titan’s ionosphere: Magnetospheric introduction of free oxygen and a source of titan’s aerosols?” pp. 1547–1557, 2009. [Online]. Available: [www.elsevier.com/locate/pss](http://www.elsevier.com/locate/pss)
- [48] M. A. English, L. M. Lara, R. D. Lorenz, P. R. Ratcliff, and R. Rodrigo, “Ablation and chemistry of meteoric materials in the atmosphere of titan,” *Advances in Space Research*, vol. 17, pp. 157–160, 1996.
- [49] P. A. Dalba and P. Withers, “Cassini radio occultation observations of titan’s ionosphere: The complete set of electron density profiles,” *Journal of Geophysical Research: Space Physics*, vol. 124, pp. 643–660, 1 2019.
- [50] E. Barth and O. Toon, “Modeling water ice clouds in titan’s 500 km haze layer,” in *AAS/Division for Planetary Sciences Meeting Abstracts# 37*, vol. 37, 2005, pp. 45–05.
- [51] V. Bronshten, *Physics of Meteoric Phenomena*, 1983, vol. 53.
- [52] E. J. Opik, *Physics of meteor flight in the atmosphere*. Courier Corporation, 1958.
- [53] F. a. Lindemann and G. M. B. Dobson, “A theory of meteors, and the density and temperature of the outer atmosphere to which it leads,” *Proceedings of the Royal Society A: Mathematical, Physical and Engineering Sciences*, vol. 102, pp. 411–437, 1 1923. [Online]. Available: <http://rspa.royalsocietypublishing.org/cgi/doi/10.1098/rspa.1923.0003>
- [54] L. Jacchia, “The physical theory of meteors. viii. fragmentation as cause of the faint-meteor anomaly,” *The Astrophysical Journal*, vol. 121, pp. 521–527, 1955. [Online]. Available: <http://adsabs.harvard.edu/full/1955ApJ...121..521J>

- [55] P. BABADZHANOV and E. KRAMER, "Some results of investigations of instantaneous meteor photographs(meteor evaporation, luminescence and fragmentation studied by instantaneous photographic exposure method noting wakes, terminal blending phenomena and successive disintegrations)," 1968.
- [56] R. Hawkes and J. Jones, "A quantitative model for the ablation of dustball meteors," *Monthly notices of the Royal Astronomical Society*, vol. 173, pp. 339–356, 1975.
- [57] K. Hornung, E. M. Mellado, O. J. Stenzel, Y. Langevin, S. Merouane, N. Fray, H. Fischer, J. Paquette, D. Baklouti, A. Bardyn, C. Engrand, H. Cottin, L. Thirkell, C. Briois, J. Rynö, J. Silen, R. Schulz, S. Siljeström, H. Lehto, K. Varmuza, A. Koch, J. Kissel, and M. Hilchenbach, "On structural properties of comet 67/p dust particles collected in situ by rosetta/cosima from observations of electrical fragmentation," *Planetary and Space Science*, p. 105747, 7 2023. [Online]. Available: <https://linkinghub.elsevier.com/retrieve/pii/S0032063323001162>
- [58] D. Subasinghe, M. Campbell-Brown, and E. Stokan, "Physical characteristics of faint meteors by light curve and high-resolution observations, and the implications for parent bodies," *Monthly Notices of the Royal Astronomical Society*, vol. 457, pp. 1289–1298, 2016.
- [59] M. Campbell-Brown and D. Koschny, "Model of the ablation of faint meteors," *Astronomy and Astrophysics*, vol. 422, pp. 751–758, 5 2004. [Online]. Available: <http://www.edpsciences.org/10.1051/0004-6361:20041001>
- [60] J. Borovička, "Properties of meteoroids from different classes of parent bodies," A. Milani, G. Valsecchi, and D. Vokrouhlický, Eds., vol. 2. Cambridge University Press, 5 2007, p. 107. [Online]. Available: [http://www.journals.cambridge.org/abstract\\_S1743921307003134](http://www.journals.cambridge.org/abstract_S1743921307003134)
- [61] D. Janches, A. A. Berezhnoy, A. A. Christou, G. Cremonese, T. Hirai, M. Horányi, J. M. Jasinski, and M. Sarantos, "Meteoroids as one of the sources for exosphere formation on airless bodies in the inner solar system," 6 2021.
- [62] J. Mathews, S. Briczinski, A. Malhotra, and J. Cross, "Extensive meteoroid fragmentation in v/uhf radar meteor observations at arecibo observatory," *Geophysical Research Letters*, vol. 37, no. 4, 2010.
- [63] D. Vida, P. G. Brown, M. Campbell-Brown, R. J. Weryk, G. Stober, and J. P. McCormack, "High precision meteor observations with the canadian automated meteor observatory: Data reduction pipeline and application to meteoroid mechanical strength measurements," *Icarus*, vol. 354, 1 2021.
- [64] M. J. Mazur, P. Brown, P. Gural, D. Vida, T. Mills, M. Campbell-Brown, and J. R. Gill, "An emccd-based meteor survey: Preliminary results and debiasing," 2023.
- [65] G. H. Duntzman, *Principal components analysis*. Sage, 1989, vol. 69.



## Bibliography

Western

- [66] T. Henych, J. Borovička, and P. Spurný, “Semi-automatic meteoroid fragmentation modeling using genetic algorithms,” *arXiv preprint arXiv:2301.11076*, 2023.